JOURNAL OF MATERIALS SCIENCE 26 (1991) 6673–6684

Wetting and interfacial reactions in Al–Li–SiC_p metal matrix composites processed by spray atomization and deposition

M. GUPTA, I. A. IBRAHIM, F. A. MOHAMED, E. J. LAVERNIA
Materials Section, Department of Mechanical and Aerospace Engineering, University of California, Irvine, CA 92717, USA

The present study addresses the wetting and interfacial behaviour in a SiC_p reinforced aluminium–lithium alloy processed by spray atomization and deposition. The microstructural characteristics of the spray atomized and deposited Al–Li–SiC_p metal matrix composites were investigated as a function of processing history and thermal exposure. The present results show that there was sufficient interfacial activity at the Al–Li/SiC interface during deposition to establish a stable bond. Furthermore, the absence of interfacial reaction products suggests that the temperature during deposition remained relatively low. When the spray deposited material was exposed to temperatures in excess of 600 °C, severe interfacial reactions and the formation of oxide phases were noted. The microstructural studies were accomplished using optical microscopy, scanning electron microscopy (with energy dispersive X-ray spectroscopy), transmission electron microscopy, and X-ray diffractometry.

1. Introduction

The attractive physical and mechanical properties that can be obtained with metal matrix composites (MMCs) have been documented extensively [1–7]. Many of the MMCs produced today, however, do not exhibit the ideal properties that would be anticipated based on the rule of mixture calculations. This behaviour has been attributed to reinforcement degradation and poor matrix-to-reinforcement bonding resulting from extensive interfacial reactions during processing [8].

Systematic studies of metal/ceramic interfaces were initiated in the early 1960s [9]. It is now widely accepted that in order to maximize interfacial bond strength in MMCs, it is necessary to promote wetting, control surface interactions, and minimize oxide formation. Wetting is effected between a metal and a liquid when the strength of the interfacial bond exceeds the surface tension of the liquid. Wetting is difficult to achieve in molten metals due to their relatively high surface tension values (60–2400 mJm^{-2}). There are, however, various techniques which can be utilized to improve the wetting characteristics of MMCs. These techniques are based on the principle that the contact angle formed in a molten metal/ceramic system can be decreased through: (a) increasing the surface energy of the solid, (b) decreasing the solid/liquid interfacial energy, and (c) decreasing the surface tension of the liquid metal. In practice, the bond formed between the matrix and reinforcement can be enhanced by [10]: (a) applying metallic coatings such as Ni and Cu to the ceramic particulates [11, 12], (b) alloying the metallic matrix with reactive materials such as Li, Mg, Ca, Ti, Zr, and P, to reduce the surface tension of the melt and/or the solid/liquid interfacial energy, and to induce chemical reactions at the interface [13–16], and (c) heat treating the ceramic particulates in order to promote desorption of adsorbed gases from the ceramic surfaces [17]. The principles underlying these practices are discussed subsequently.

Wetting can be promoted in certain metal/ceramic systems through additions of elements which have a high affinity for oxygen, such as elements in groups I and II of the periodic table, e.g., Li and Mg in aluminium alloys [13, 14]. These elements segregate to the interfacial region and weaken any oxide layers present [18]. For the case of Mg additions to aluminium, for example, additional improvements in wetting behaviour result from a decrease in surface tension, as a result of the low surface tension of Mg (0.599 N/m) relative to that of aluminium (0.760 N/m). The addition of 3 wt % Mg to Al reduces the surface tension from 0.760 to 0.620 N/m [15]. Furthermore, the addition of reactive elements to the melt can also enhance wetting by promoting interfacial reactions. For example, chemical reactions have been observed to occur readily between Al_2O_3 and divalent transition metal oxides to form aluminate spinels such as $MgO \cdot Al_2O_3$ [16]. Such mineral spinels or oxides promote interfacial bonding, since they form strong bonds between both metals and ceramics.

From the above discussion, it is apparent that some interfacial activity will be beneficial to the wetting behaviour of MMCs. In the presence of high processing temperatures, however, extensive interfacial

0022–2461/91 $03.00 + .12

reactions with concomitant degradation in the metal/ceramic bond will have an adverse effect on mechanical behaviour. Hence, the formation of extensive interfacial reactions must be avoided and the thermodynamic activity of certain elements during processing must be controlled. In the Al/SiC system, for example, intermediate phases such as Al_4C_3 and Al_4SiC_4 may form during thermal exposure either as a continuous layer or isolated precipitates [19]. At temperatures above the melting point of Al, SiC reacts with molten Al according to the following reactions

$$4Al + 3SiC = Al_4C_3 + 3Si \quad (1)$$

$$4Al + 4SiC = Al_4SiC_4 + 3Si \quad (2)$$

In the case of reaction 1, further growth of the reaction products occurs by solid state diffusion through the formed Al_4C_3 layer. In the case of reaction 2, however, the reaction continues by the dissolution of the SiC into the molten Al matrix. It is important to note, however, that the presence of Al_4SiC_4 phase has not been confirmed experimentally. Although the bond formed between the SiC and Al_4C_3 is generally strong, the topology of the resulting Al_4C_3–SiC interface can be highly irregular when the original interface is irregular, or if there is dissolution/growth reaction between SiC and liquid Al. The irregular topology of the interface may promote stress localization during deformation. This is best exemplified in the C(graphite)/Al system, where the presence of cracks, cavities and voids, formed at the C/Al_4C_3 interface introduces additional mechanisms of crack nucleation and propagation, relative to those active in the unreinforced metal [20]. In addition to extensive interfacial reactions, high processing temperatures will promote oxide formation and segregation of the constituent elements [20–22]. Segregation of elements such as Cu and Mg from grain interiors will promote localized corrosion, and limit precipitation–hardening mechanisms.

The various processing techniques which have developed to fabricate MMCs can be classified as: (a) liquid phase processes, (b) solid phase processes, or (c) two-phase processing methods. Liquid phase processes involve the casting of a mixture of liquid–matrix and ceramic particulates. These include the DURAL process [11, 23] and melt infiltration processes [24–27]. Solid phase processes include the oxidation of a melt/reinforcement mixture (e.g., the Lanxide™ Process [28]) and powder metallurgy (PM) (blending and consolidation of alloy matrix powders with reinforcement particulates) techniques [11, 29]. Although liquid phase processes and solid phase processes have been carried out to various degrees of success, there is ample experimental evidence suggesting that there are some important drawbacks [25, 30, 31]. More recently, two-phase processes have been successfully utilized to process particulate reinforced MMCs with minimal reactivity; these include rheocasting [32, 33], and spray atomization and deposition processes [34–38]. A review of the available literature on particulate reinforced MMCs may be found elsewhere [39].

Although the results of recent studies [34–40] suggest that spray atomization and deposition processes can be successfully utilized to incorporate ceramic reinforcements into a metallic matrix with minimal reactivity, there exists no information on the mechanisms affecting the wetting behaviour of the reinforcements during processing. The objective of the present study was to provide insight into the wetting and interfacial behaviour of Al–Li–SiC_p MMCs processed by variable co-deposition of multiphase materials (VCM), a spray atomization and deposition technique, with particular emphasis on wetting characteristics and interfacial reactions.

2. Experimental procedure

2.1. Material

Reynolds Metals Company provided the aluminium–lithium master alloy as cast ingots, 100 mm × 200 mm × 600 mm. The ingots were inspected for major defects, and chemically analysed in preparation for atomization. The chemical analysis of the remelted alloy was Al–2.1 wt % Li. The selection of an Al–Li binary alloy (solid solution) as a matrix material was prompted by the results of Wolf *et al.* [14] and Delannay *et al.* [15]. Their work indicates that lithium enhances the wettability of ceramic particulates by molten metals by segregating to the interfacial region and weakening any oxide layers present. In addition, lithium effectively reduces the density and increases the modulus of the MMCs [40].

The SiC particulates were obtained from the Superior Graphite Company. The size distribution of the SiC particulates (β phase) was Gaussian and exhibited an average of 3 μm (d_{50}). In addition, 90% of the distribution of SiC particulate sizes was less than 5 μm (d_{90}) with 10% of the distribution falling under 1 μm. Overall, most of the SiC particulate sizes (99%) were under 15 μm. The bulk and particulate density was 0.78 and 3.1 g/cm^3, respectively. In order to ensure moisture desorption from the surface of the particulates, these were vacuum degassed at 800 °C for 30 minutes prior to the experiments.

2.2. VCM processing

During VCM, the matrix material is disintegrated into a fine dispersion of droplets using high-velocity inert gas jets (see Fig. 1). Simultaneously, one or more jets of strengthening phases are injected into the atomized spray at a previously determined spatial location. This location is determined on the basis of numerical analysis of the fraction solid contained in the atomized matrix, as a function of flight distance; a more thorough discussion of the numerical results and injection details is presented elsewhere [34, 35]. The objective is to achieve interfacial control by injection of the reinforcing particulates at a spatial location where the atomized matrix spray contains a limited amount of volume fraction liquid. In this manner, contact time, thermal exposure of the reinforcing particulates to the partially solidified matrix, and interfacial reactions can be minimized. In order to avoid extensive oxida-

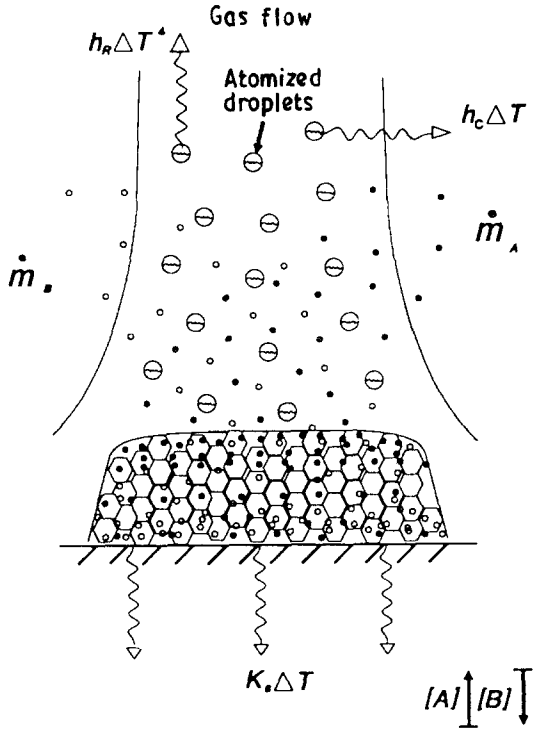

Figure 1 Schematic diagram of VCM technique.

tion of the Al–Li matrix during processing, the experiments were conducted inside an environmental chamber. The latter was evacuated down to a pressure of 150 micrometres of Hg, and backfilled with inert gas prior to melting and atomization.

Five VCM experiments were conducted for this study. The primary experimental variables used during each experiment are listed in Table I.

2.3. Structural characterization

In order to study the resulting microstructure and phases, metallographic samples were prepared from various locations in the as-spray deposited Al–Li–SiC_p MMCs. The microstructural studies were conducted: (a) on the as-spray deposited material, and (b) on the as-spray deposited material after two isochronal anneals at preselected temperatures. The details of the thermal exposure are given in Table II.

In addition, some of the as-spray deposited materials were machined into a square prism, of cross-section $1.0 \times 1.0\ cm^2$, and fractured at room temperature. The resulting fracture surfaces were then analysed.

The heat treatment temperature of 600 °C shown in Table II was selected on the basis of the Al/SiC phase diagram (see Fig. 2). As shown in this figure, formation of the Al_4C_3 phase is thermodynamically stable at this temperature.

The microstructural characterization was accomplished using optical microscopy, transmission electron microscopy (TEM), scanning electron microscopy (SEM) with energy dispersive X-ray spectroscopy (EDS), and X-ray diffractometry (XRD).

2.3.1. Optical microscopy (OM)

Optical microscopy was conducted on polished and etched, as-spray deposited samples using conventional and differential interference contrast (DIC) techniques. The size, volume fraction and distribution of the SiC particulates was characterized from the optical micrographs using a Buehler Omnimet II Image Analyser.

2.3.2. Transmission electron microscopy (TEM)

Transmission electron microscopy was performed on a JEOL 100 C at an operating voltage of 100 kV. The TEM specimens were prepared by sectioning and mechanical polishing into thin foils of about 0.1–0.5 mm in thickness. The foils were then chemically polished to perforation, using the window technique in a 1:2 solution of HNO_3 and methanol at approximately −20 °C and a voltage of approximately 10 V.

2.3.3. Scanning electron microscopy (SEM)

SEM studies were conducted using a HITACHI S-500 microscope. The samples were cut to a thickness of 0.5 cm and mirror polished using conventional techniques. The polished samples were then examined in secondary electron mode for microstructural details;

TABLE I Experimental variables used in study

Variables	Experiment number				
	1	2	3	4	5
Matrix alloy	Al–Li	Al–Li	Al–Li	Al–Li	Al–Li
Reinforcement	SiC_p	SiC_p	SiC_p	SiC_p	SiC_p
Atomization pressure	1.2 MPa	1.2 MPa	1.2 MPa	1.2 MPa	1.2 MPa
Atomization gas	Argon	Argon	Argon	Nitrogen	Nitrogen
Fluidized bed gas	Argon	Argon	Argon	Argon	Nitrogen
Injection angle[a]	30°	20°	90°	30°	30°
Injection distance	0.14 m	0.13 m	0.15 m	0.14 m	0.14 m
Fluidizing pressure	0.69 MPa	0.69 MPa	0.69 MPa	0.69 MPa	0.69 MPa
Flight distance 0.41 m	0.41 m	0.41 m	0.41 m	0.41 m	0.41 m
Pouring temperature	840°	840°	840°	840°	840°
Metal delivery tube Diameter	3.30 mm	3.27 mm	3.33 mm	3.05 mm	3.00 mm
Atomization nozzle Pressure condition[b]	~0	6.0 kPa	~0	~0	~0

[a] The injection angle refers to the relative angle between the spray of SiC_p and the concentric vertical axis of the atomized matrix.
[b] Positive and zero values represent pressurization and metal free-fall, respectively.

TABLE II Specimen thermal history

Designation	Conditions
Htl	as-spray deposited condition
Ht2	as-spray deposited + heat treated at 600 °C for 2 hours
Ht3	as-spray deposited + furnace re-melting under a flow of argon atmosphere at 870 °C for 1 hour.

point analyses were carried out at selected regions of the sample surface to detect the presence of reaction products. SEM/EDS analyses were also conducted on as-deposited and fractured Al–Li–SiC_p specimens in order to avoid surface contamination during metallographic preparation. The exposed SiC particulates on the fracture surface were then analysed by varying the accelerating electron voltage (10, 15, 20, and 25 keV) and measuring the intensity of the Al and Si X-ray peaks at different depths throughout the thickness of the particulates.

2.3.4. X-ray diffraction (XRD)

X-ray diffraction analysis was conducted on spray deposited samples in the Ht1 and Ht3 conditions (see Table II). Thin samples were exposed to CuK_α radiation ($\lambda = 15.418$ nm) using a scanning speed of 2 deg/min. A plot of intensity versus 2θ was obtained, illustrating peaks at different Bragg angles. The Bragg angles corresponding to different peaks were noted and the values of interplanar spacings, d, was calculated from Bragg's law ($\lambda = 2d \sin\theta$). The values of d obtained were then matched with standard values for aluminium and other phases.

3. Results

3.1. Structural characterization

The as-spray deposited VCM materials exhibited a discoidal geometry, 50 mm in height by 150 mm in diameter. The height of the deposits decreased from a maximum of 50 mm at the centre, to a minimum of 5 mm towards the periphery. The density of the as-spray deposited VCM materials ranged from 2.4 g/cm^3 to 2.6 g/cm^3. These density values correspond to approximately 88–97% of the theoretical density, as computed for an Al–Li–5 vol % SiC_p material.

3.2. Optical microscopy (OM)

Optical microscopy was conducted on coupons of the VCM Al–Li/SiC_p material; one example is shown in Fig. 3a. This figure reveals the presence of an equiaxed grain morphology with an average grain size of 65 μm. This grain morphology has also been reported by other investigators [41–43]. The average grain size for experiments 1 to 5 was in the range of 66–71 μm; the as-cast Al–Li grain size was 207 μm. Optical micrographs of the deposits were taken using differential interference contrast (DIC); one example is shown in Fig. 3b. The use of the DIC technique facilitated the identification of the distribution of the SiC particulates in the matrix.

3.3. Image analysis

Image analysis was conducted on a number of samples taken from experiments 1–5 in order to characterize the size, distribution and location of SiC_p in the Al–Li matrix. The size and distribution of SiC_p obtained from the image analysis were then used to compute the interparticle spacing of SiC_p according to the formula discussed by Nardone and Prewo [7]:

$$\lambda = (l_1 l_2 / f)^{1/2} \quad (3)$$

where l_1, l_2 and f are the length, breadth, and the volume fraction of the SiC_p, respectively. The results of image analysis and the computed values of interparticle spacings, λ, are shown in Table III.

3.4. Transmission electron microscopy (TEM)

Transmission electron microscopy studies were conducted on samples of the VCM materials in the Ht1, Ht2 and Ht3 conditions (see Table II). A representative view of the as-spray deposited Al–Li–SiC_p microstructure is shown in Fig. 4. This figure shows the

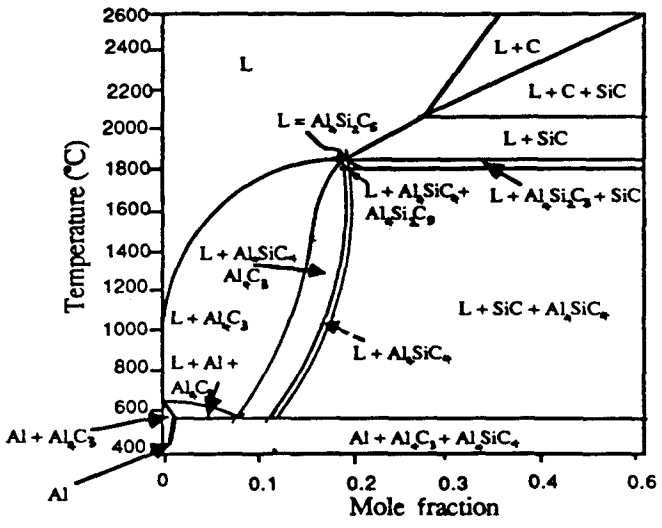

Figure 2 Phase diagram of Al–SiC system [19].

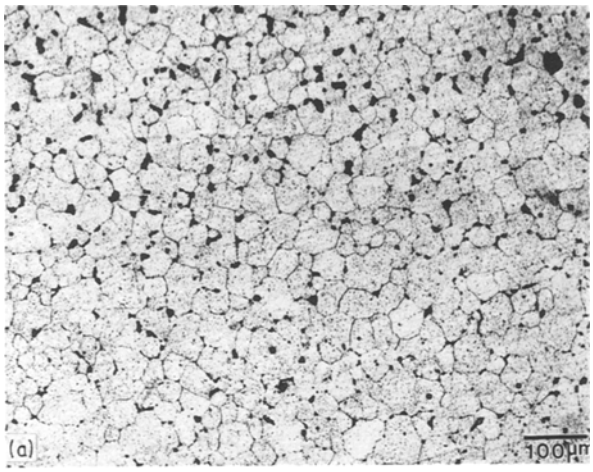

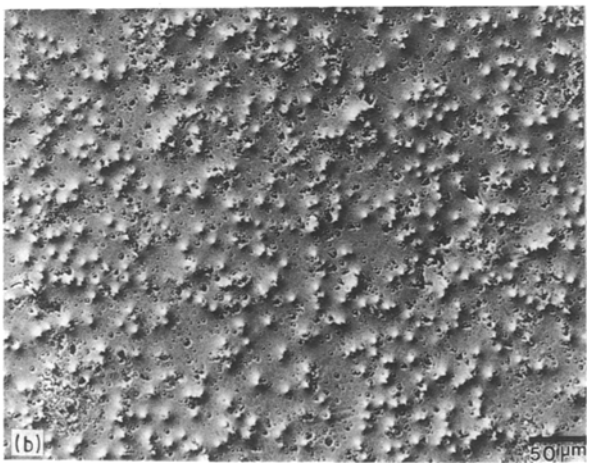

Figure 3 Optical micrograph showing: (a) the grain structure of the VCM deposit, and (b) SiC_p distribution in the matrix.

presence of a highly irregular Al–SiC interfacial region. In some regions of the TEM samples, the particulates could be seen suspended by thin ligaments of the matrix across narrow interfaces. In addition, a high dislocation density in the matrix region surrounding the particulates was also noted (See Fig. 4).

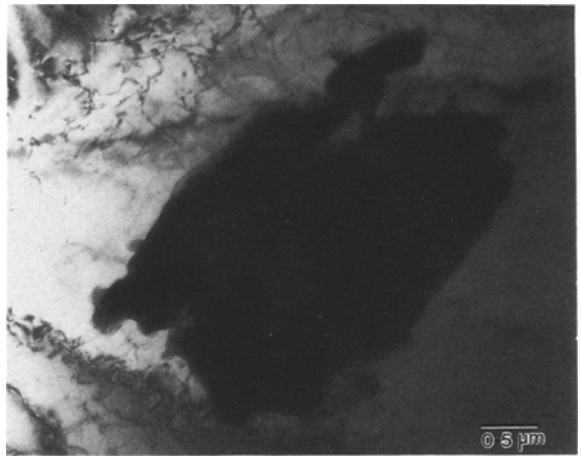

Figure 4 Representative TEM micrograph of the Al–Li–SiC_p in the Ht2 condition.

3.5. SEM/EDS

Scanning electron microscopy of samples removed from the as-spray deposited Al–Li–SiC_p materials revealed the presence of a finite amount of non-interconnected porosity. The micrometre-size pores were randomly located throughout the microstructure, and exhibited a near elliptical morphology. The distribution of pores was found to be bimodal, with a large proportion in the 1–2 μm and 10–20 μm size ranges; the volume fraction of porosity was estimated to be approximately 3–12 % throughout the material.

Representative SEM micrographs of the deposited Al–Li–SiC_p MMCs are shown in Fig. 5 for the Ht1 and Ht3 conditions. Fig. 5a illustrates the morphology of the fractured surface corresponding to a sample in the Ht1 condition. The surfaces of the particulates shown in Fig. 5a exhibit an irregular, faceted morphology. Detailed examination of the fracture surface revealed that particulate fracture, rather than pullout, during deformation, suggesting a strong interfacial bond. Fig. 5b shows the extensive interfacial reaction

TABLE III Results of image analysis of Al–Li–SiC_p composite

Sample number[a]	Equivalent diameter (μm)[b] Min.	Max.	Mean	σ	Volume fraction (%) Min.	Max	Mean	σ	Interparticle spacing (λ, μm)
1 A	0.57	09.00	2.70	2.01	1.92	08.33	3.49	1.82	14.48
1 B	0.57	10.00	2.71	2.10	2.89	06.15	4.56	1.13	12.69
1 C	0.57	12.00	2.10	1.76	4.40	13.44	7.89	1.91	07.48
2 A	----NOT DETERMINED----					–	9.60	–	08.71[d]
2 C	----NOT DETERMINED----					–	11.65[c]	–	07.91[d]
3 A	0.57	11.00	2.76	2.13	4.69	7.19	6.12	0.85	11.14
3 B	0.57	10.00	2.86	2.12	4.38	6.10	5.13	0.50	12.62
3 C	0.57	9.00	3.34	2.16	1.34	3.16	2.49	0.54	21.16
4 A	0.25	13.56	1.65	2.92	18.39	24.72	20.75	2.25	18.14
4 B	0.25	9.33	1.54	2.34	3.17	07.36	05.41	1.56	25.71
5 A	0.25	10.68	1.61	2.79	2.60	07.63	03.70	1.54	19.99
5 B	0.25	16.95	2.27	4.24	2.77	08.95	06.00	2.29	11.89
5 C	0.25	18.92	2.58	4.83	0.76	15.00	05.29	5.23	10.78

[a] A, B, C designations refer to top, centre and bottom regions, respectively, of the spray deposited Al–Li–SiC_p.
[b] The equivalent diameter is a measure of the size of the SiC particulates.
[c] These values of the volume fraction were determined using quantitative metallography.
[d] These values were computed from Equation 3 for a SiC_p size of 2.7 μm.

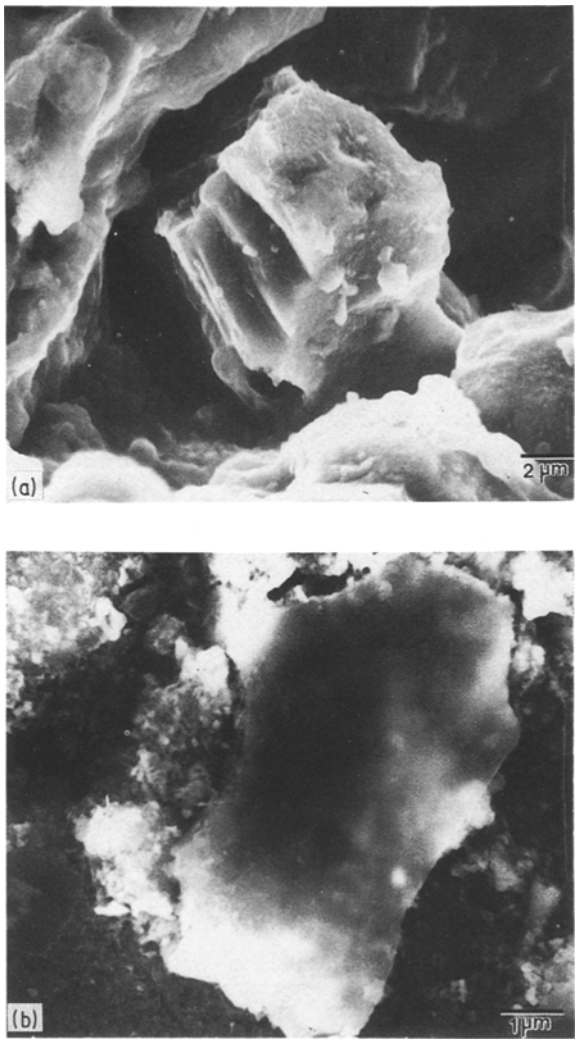

Figure 5 Representative SEM micrograph showing: (a) the fractured surface of the as-deposited Al–Li–SiC_p, and (b) the presence of reaction products in the remelted Al–Li–SiC_p material (Ht3 condition).

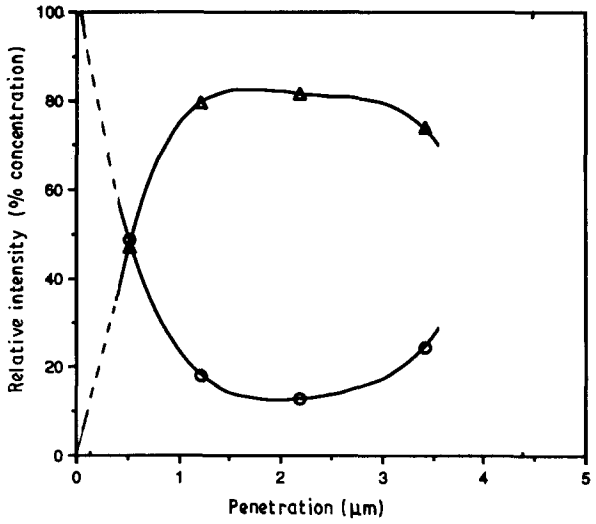

Figure 6 Concentration of Al and Si as a function of penetration in the SiC_p for the as-spray deposited VCM material. (○) Al; (△) Si.

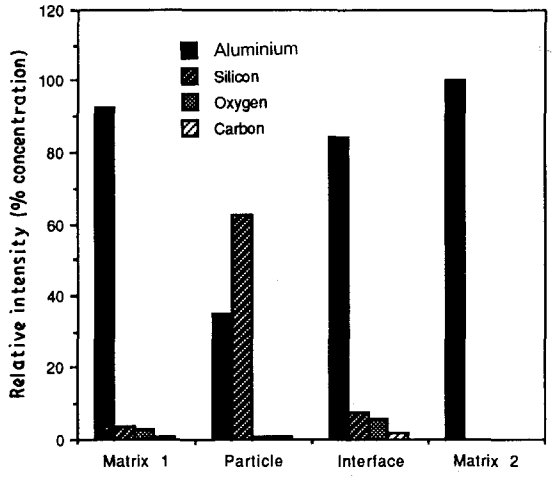

Figure 7 Histogram of the Al–Li–SiC_p material in the Ht3 condition showing the relative intensities of SEM/EDS signals for Al, Si, O, and C. The Matrix 1 and Matrix 2 designations refer to EDS analyses conducted on the matrix at distances of 2 and 10 μm, from the interface, respectively.

which occurs between the SiC particulates and the Al–Li matrix during remelting of the Al–Li matrix (Ht3 condition).

The results of EDS analyses conducted on the as-spray deposited material (Ht1 condition) are shown in Fig. 6. The results shown in this figure correspond to the location shown in Fig. 5a. The relative concentrations of the constituent elements were calculated from the intensity of the X-ray beam, and are plotted in Fig. 6 as a function of depth of penetration into a SiC particulate. The depth of penetration, R, of an electron beam into a SiC particulate was computed from [44]:

$$R = (4120/\rho)E^n \quad (4)$$

where $n = 1.265 - 0.0954 \ln E$, E = primary electron energy (in MeV), and ρ = density of absorbing media (in g/cm^3). The results obtained using Equation 4 show that the accelerating voltages used in the present study, namely 10, 15, 20, and 25 keV, correspond to penetration depths of 0.519, 1.218, 2.189, and 3.413 μm, respectively.

Finally, the relative concentrations of the constituent elements corresponding to the location shown in Fig. 5b, (Ht3 condition), are shown in Fig. 7. The results shown in Fig. 7 show that the Al/SiC interface contains O, C, Si and Al. In this figure, the location designated as Matrix 1 refers to a region approximately 2 μm from the interface, whereas location designated as Matrix 2 was approximately 10 μm away from the interface.

3.6. X-ray diffraction (XRD)

The X-ray diffraction spectra corresponding to samples in the Ht1 and Ht3 conditions were analysed. The lattice spacings (d) corresponding to the observed Bragg angles are shown in Table IV. Also included in this table are the standard lattice spacings corresponding to pure Al, SiC, Al_4C_3, AlSiC, Al_2O_3 and Al_2Mg_3. The XRD spectrum corresponding to the as-spray deposited Al–Li–SiC_p material (Ht1) indicates the presence of pure aluminium. The XRD spectrum corresponding to the re-melted Al–Li–SiC_p material (Ht3), however, exhibits additional peaks. Inspection

TABLE IV Results of X-ray diffractometry studies

Htl sample								
Angle	36.4	39.0	45.3	54.6	60.6	65.8	78.8	82.9
Calculated *d* values	–	2.36	2.00	–	–	1.42	1.21	1.16
Band size (%)	–	60	100	–	–	15	21	10
Ht3 sample								
Angle	36.4	39.0	45.3	54.6	60.6	65.8	78.8	82.9
Calculated *d* values	2.47	2.36	2.00	1.68	1.53	1.42	1.21	1.16
Band size (%)	10	100	59	5	5	36	35	13
Standard *d* values								
Al	2.338	2.025	1.432	1.221	1.169			
Al_2O_3	2.379	1.601	1.510					
Al_2Mg_3	2.48	1.60	1.52					
Al–Li	2.26	1.92	1.58					

of Table IV suggests that these additional peaks correspond to Al_2O_3. The absence of X-ray peaks corresponding to SiC, Al_4C_3 and AlSiC phases was thought to result from the relatively low volume fraction of SiC particulates present in the samples utilized for the XRD study (see Table III).

4. Discussion

4.1. Grain structure

The experimental results show that the grain morphology of the VCM material is equiaxed; this observation is in agreement with previous findings [41–43, 45]. It has been proposed [46] that the formation of an equiaxed grain morphology during spray deposition is associated with three simultaneous processes: (1) dendrite arm fragmentation, (2) nucleation/grain multiplication, and (3) constrained growth. During deposition, there is extensive fragmentation of the dendrite arms formed during solidification, as a result of the repeated impact of the partially solidified droplets, first with the deposition surface, and subsequently, with each other. The presence of dendrite fragments, the development of strong convective currents in the liquid during impact, and the formation of a large number of solid nuclei have all been proposed as factors which contribute towards the development of an equiaxed grain morphology during spray atomization and deposition. A more thorough discussion of these mechanisms can be found elsewhere [46].

Comparison of the grain size of the spray deposited Al–Li binary alloy to that of the VCM Al–Li–SiC_p material indicates that the presence of the SiC particulates effectively reduces the grain size by approximately 10%. The finer grain morphology of the Al–Li–SiC_p is thought to result from a combined effect of three distinct mechanisms: enhanced heat transfer, increased solidification prior to impact, and grain boundary pinning effects. During flight, the SiC particulate spray from the fluidized bed effectively enhances the convective heat transfer from the matrix droplets as a result of its lower temperature (the particulates are injected into the matrix spray at room temperature) and high relative velocity. The high relative velocity between the atomized droplets and the SiC_p carrier gas is a direct result of the injection angle (see Table I). Further work is in progress in this area in order to develop an understanding of the effects of the reinforcements on the resulting microstructure during spray deposition.

Regarding the presence of pores in the as-spray deposited VCM material, the observed irregular morphology of the pores suggests that porosity develops from interstices formed as droplets impact on one another. This is consistent with the findings of other investigators [41–43]. A discussion on the origin of porosity in spray deposited materials can be found elsewhere [35, 46].

The high dislocation density observed in the Al–Li matrix adjacent to the SiC particulates is in agreement with previous findings [43, 47]. The high dislocation density observed in MMCs is thought to result from the large difference in coefficient of thermal expansion (CTE) of Al and SiC (10:1) which causes thermal mismatch strains, ε, between reinforcement and matrix during solid state cooling. These strains are relaxed by the formation of a dislocation network, which in turn, will alter the response of the MMC to thermomechanical processing, relative to that of unreinforced alloys [19, 47, 48].

4.2. SiC particulate size and distribution

The results shown in Table III indicate variations in the volume fraction of SiC_p with spray deposited thickness. Regarding variations in volume fraction of SiC_p for a single experiment, the results shown in Table V do not reveal a clear correlation between spray deposited thickness, the amount of SiC_p, and the experimental conditions (see Table I). Although a systematic investigation of the effects of the injection angle on the distribution of SiC_p in the matrix was outside the scope of the present study, the variations in volume fraction with spray deposited thickness are most likely affected by changes in the fluidization conditions (i.e., pressure drop) and mass flow rate of the metal during the experiments, in addition to the injection angle. Furthermore, since the volume fraction of SiC_p was determined using image analysis, the results should be treated as an order of magnitude approximation of the actual SiC_p volume fraction. The results do suggest, however, that it is possible to alter the resulting variations in volume fraction of SiC particulate through changes in the fluidization condi-

TABLE V Numerical model results of the thermal history of the droplets of varying sizes

Diameter of droplet (μm)	Temperature (°C) (at 0.14 m)	f_s (%)	Temperature (°C) (at 0.41 m)	f_s (%)	Thickness of oxide film (nm)	Oxide film (0.14 m)[a]	Oxide film (0.41 m)[a]
25	182	100	100	100	23.4	$Al_2O_3 3H_2O$/ $Al_2O_3H_2O/Li_2O$	$Al_2O_3 3H_2O$/ $Al_2O_3H_2O/Li_2O$
62	605	95	472	100	58.5	γ-Al_2O_3/ γ-$LiAlO_2$	$Al_2O_3 H_2O$/ γ Al_2O_3
156	650	33	647	48	140	γ-Al_2O_3/ γ-$LiAlO_2$	γ Al_2O_3/ γ $LiAlO_2$

[a] The type of oxides shown for the indicated temperatures and droplet sizes are for equilibrium conditions, and were determined from the work of [61, 62] on the basis of the average temperature of the droplet.

tions. The higher volume fraction of SiC particulates observed for experiment 2 was thought to result from a pressurization condition at the metal delivery tube (see Table I). This behaviour, which is caused by the relative position of the metal delivery tube to the gas jets, has been studied extensively [49]. In the present study, the pressurization effect reduced the metal flow rate of the matrix, effectively decreasing the Al–Li/SiC particulate mass flow ratio, hence resulting in a higher SiC particulate concentration.

Regarding the size distribution of the SiC_p, the results from Table III ($d_{50} = 2.7$ μm) are consistent with the initial SiC_p size ($d_{50} = 3.0$ μm). The slight reduction in particulate size can be attributed to the difficulties associated with fluidizing the coarse SiC particulates. The results also indicate that the processing methodology does not favour clustering of the SiC particulates.

In terms of the location of the SiC_p in the matrix, comparison of the computed interparticle spacings from Table III to the resulting grain sizes, indicates that the particulates were randomly distributed in the matrix (i.e. not preferentially located at the grain boundaries). This was also confirmed through SEM analysis. After impact with the substrate, retention of a suitable particulate dispersion throughout the matrix is facilitated by the presence of primary dendrite debris resulting from droplet impact. The mechanisms affecting the distribution of SiC_p during VCM are discussed in the subsequent section.

4.3. Wetting and interfacial reactions

In order to discuss the wetting behaviour during VCM, it is necessary to review the current understanding of the factors which govern the behaviour of liquid/solid interfaces under equilibrium condition.

A concept commonly used to measure the adhesive strength between a solid and liquid interface is the work of adhesion W_{ad}, defined by the Young–Dupré equation as:

$$W_{ad} = \gamma_{1g}(1 + \cos\theta) \quad (5)$$

W_{ad} has been defined [15, 18] as the work required to separate a unit area of the solid/liquid interface; γ_{1g} is the liquid/gas interfacial energy. Wetting of a solid surface by a liquid is achieved when $\cos\theta > 0$, that is when $\gamma_{sg} > \gamma_{s1}$; where γ_{sg} and γ_{s1} are the solid/gas and solid/liquid interfacial energies, respectively. Moreover, it can be shown [15] that wetting will occur when the driving force for wetting D_f exceeds the liquid interfacial energy, i.e.

$$D_f \geq \gamma_{1g} \quad (6)$$

The driving force for wetting, D_f, is governed by two factors: the surface tension of the liquid, and the strength of the liquid/solid interaction at the interface [15]. In turn, these two factors are affected by variables such as interfacial reactions, surface characteristics, heat of formation, valence electron concentration, temperature and time [50]. For molten metals, it is difficult to satisfy Equation 6, because metals typically exhibit rather high surface tension values (64–2400 mJm^{-2}). Hence, the wettability of oxides by molten metals is generally poor. Recent results suggest that the wettability of molten metals against ZrO_2 [15] and Al_2O_3 [51] is approximately proportional to the free energy of oxide formation of the metal. In the presence of oxygen, however, metals with a high free energy of oxide formation form stable oxides which act as effective diffusion barriers that decrease the level of interaction at the interface. Furthermore, the absorption of oxygen from the atmosphere can also be detrimental to the wetting behaviour by decreasing γ_{sg}. As a result, wetting is not observed in molten metal/ceramic systems until a certain threshold temperature is achieved which allows penetration of the molten metal through the oxide layer. For example, Laurent *et al.* [52] and Warren and Anderson [53] attributed the transition from non-wetting to wetting behaviour in Al/SiC system to the disappearance of the oxide layer from the molten Al droplet. Furthermore, Warren and Anderson [53] also singled out the destabilization of the oxide layer (by the presence of reactive elements) and the improvement of interfacial reaction kinetics with temperature as the main factors contributing to wettability.

Even in systems that exhibit a strong driving force promoting chemical reactions, the presence of oxides can prove detrimental to the wetting behaviour. In SiC/Al, for example, the high value of the work of adhesion (W_{ad} = 1000–1200 mJm^{-2}) [15], indicates that there is a strong tendency for chemical interaction at the interface. However, wetting in this system is hindered not only by the formation of Al_2O_3 on the molten metal, but also by the formation of SiO_2 on the surface of the SiC particulate. In the presence of SiO_2 and Al_2O_3, the contact angle formed between Al at its

melting point and SiC can be extrapolated [53] to be approximately 155° which corresponds to non-wetting behaviour. Under these conditions, the value of work of adhesion calculated using the method discussed by Delannay *et al.* [15] is 98.37 mJ/m^2. The latter also suggests non-wetting between the Al and SiC since the work of adhesion, W_{ad}, must be greater than the liquid/gas interfacial energy, γ_{lg} (1050 mJm^{-2}) for wetting to occur.

The wetting characteristics and the extent of interfacial activity during VCM are affected by the thermal conditions of the matrix during reinforcement injection and deposition. During VCM, the thermal and solidification conditions of the droplet distribution will depend on: (a) the thermodynamic properties of the matrix material, such as (i) liquidus temperature, (ii) solidus temperature, (iii) melting temperature, (iv) density, (v) thermal conductivity, (vi) surface tension, (vii) heat capacity, and (viii) heat of fusion; (b) the thermodynamic properties of the atomization gas such as (i) density, (ii) heat capacity, (iii) viscosity, and (iv) thermal conductivity; (c) the characteristics of the reinforcement phase(s) such as (i) size distribution, (ii) mass flow rate; and (d) the processing parameters such as (i) atomization gas pressure, (ii) nozzle/substrate flight distance, (iii) metal/gas flow ratio, and (iv) reinforcement injection. For processing conditions typical for aluminium alloys, the droplet distribution during reinforcement injection and subsequently during impact is made up of solid powders (d_{16} = 20–45 μm, $f_s \sim 1$), droplets with mostly liquid phase (d_{84} = 150–250 μm, $f_s \sim 0$), and a substantial fraction of powders in the mushy state (d_{50} = 50–90 μm, $f_s \sim 0.5$) (the subscripts 84, 50 and 16 in d_{84}, d_{50} and d_{16} represent 84%, 50% and 16% of the size distribution under this particle size) [46, 54]. As a result, during impact with the deposition surface, the SiC particulates will be surrounded by either: (a) dendrite fragments, (b) fully solidified fine droplets, or (c) liquid phase. This event is shown schematically in Fig. 8.

The presence of either dendrite fragments and/or fully solidified droplets will promote mechanical entrapment of the SiC particulates during deposition. The highly irregular surface morphology of the SiC_p, which was evident from SEM observations (see Fig. 5), will facilitate mechanical entrapment of the particulates during deposition. In related studies, Mehrabian *et al.* [55] showed that during stir casting of an Al–Si–Fe alloy containing SiC or Al_2O_3 particulates, the presence of primary dendrite debris prevents settling, flotation, or agglomeration of the ceramic particulates. The presence of either dendrite fragments and/or pre-solidified droplets during deposition will have a similar effect to that present during stir-casting. Furthermore, the presence of small crevices in the surface of the SiC particulates increases the effective surface area available for interfacial activity, and enhances the mechanical bond formed between the particulate and matrix. In the presence of pre-solidified droplets, however, the interparticle spacing will be limited by the droplet size. This is supported by the results shown in Table III, for samples 3C and 4B. The interparticle spacings computed for these two

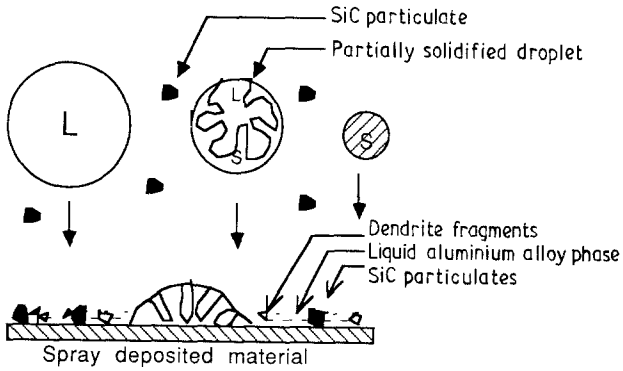

Figure 8 Schematic diagram showing the stages during impact of droplets and SiC particulates at the deposition surface.

samples, 21.2 and 25.7 μm, respectively, approach the value of the d_{16} droplet diameter, where d_{16} = 30 μm. A more thorough discussion on particulate entrapment during VCM can be found elsewhere [34, 35].

Regarding the interaction of SiC particulates with the molten Al–Li matrix during VCM processing, the preliminary results found in this investigation indicate that the temperature during deposition was sufficient to promote the formation of a stable bond, but remained sufficiently low to avoid extensive interfacial activity. The presence of a strong Al–Li/SiC bond is supported by the SEM results which showed fracture rather than pullout of SiC particulates during deformation. Furthermore, the results shown in Fig. 6 suggest that the temperature during deposition promoted some diffusion of Al into the SiC. Regarding the diffusion of Al into the SiC, the present results are apparently unexpected since previous studies have shown that the calculated mean diffusion rate of Al in SiC at 500 °C will be less than 0.1 nm/year [56]. It is worthwhile noting, however, that the present results are consistent with the findings of other investigators who have also reported diffusion of matrix elements into the reinforcing phases. Nourbakhsh *et al.* [57], for example, observed extensive diffusion of Ti into Al_2O_3 reinforcing fibres. In that study, approximately 1 wt% Ti was added to a Ni_3Al (Ni–Al–Cr–Zr–B) matrix in order to enhance wetting of the reinforcing fibres. In related studies, J. M. Yang *et al.* [58] also reported diffusion of Ni into SiC fibres in a nickel aluminide (Ni_3Al) matrix. In view of these results, and the fact that the atomic radius of Al is small, relative to that of Ti, the diffusion of Al into the SiC observed in the present study is not unexpected. Furthermore, the presence of a dislocation network at the SiC/Al interface (see Fig. 4) will most likely enhance the diffusion of Al into the SiC.

The presence of small amounts of C detected near the interface of the as-spray deposited material after heating to 600 °C for two hours (Ht2 condition) suggests the diffusion of free carbon (~0.60 wt%) from the SiC particulates thus resulting in an increase in the activity of carbon as also discussed in the related studies by Kannikeswaran and Lin [59]. Although interfacial reaction layers were not observed in the Ht1 specimens, the interfacial reaction layers were appreciably large, with thicknesses of the order of 5 μm, in the Ht3 specimen. This is consistent with the EDS results

from Fig. 7, which indicate the presence of high levels of C and O at the interface, relative to the matrix. Furthermore, this is in agreement with earlier observations [19] which suggest that fast reactions occur between SiC and molten aluminum to form carbide phases such as Al_4C_3 and Al_4SiC_4 [18, 19, 47, 48]. In the related studies, Iseki *et al.* [60] reported the presence of a thin reaction layer about 10 μm in thickness for the sintered SiC and aluminium block heat treated at 1100 °C in a vacuum of 10^{-2} Pa.

5. Dynamic wettability

The results discussed in the previous section suggest, first, that a strong interfacial bond was established between the Al matrix and the SiC particulates and second, that prolonged thermal exposure of the as-spray deposited material resulted in the formation of a reaction layer consisting primarily of carbon-containing phases, such as Al_4C_3. The presence of a strong interfacial bond and the ensuing interfacial reactions during thermal treatment are indicative of wetting of the SiC by the Al–Li matrix. In view of the fact that the interaction of the Al–Li matrix with the SiC particulates during VCM will take place under extremely non-equilibrium conditions, it is unlikely that Equations 5 and 6 may be used to predict wetting behaviour, since these equations were developed for highly equilibrium conditions. One approach that may be utilized to provide insight into the wetting behaviour during VCM is to consider the solidification conditions of the matrix droplets during co-injection, and subsequently, during deposition.

In order to determine the effect of the thermal conditions of the matrix droplets on the wetting behaviour of the SiC particulates, an enthalpy model developed elsewhere [34, 35] was used in the present study to calculate the temperature and fraction solid of the droplets, as a function of the flight distance. The numerical results are summarized in Table V for three droplet sizes: 25 μm, 62 μm and 156 μm. These three droplet sizes represent d_{16}, d_{50} and d_{84} of the droplet size distribution used in the present study, and hence can be used to gain some insight into the behaviour of the entire population of droplet sizes. In addition, the results shown in Table V were computed for two flight distances: (a) the reinforcement injection point, and (b) the deposition point.

The range of temperatures and fraction solids shown in Table V do not suggest wetting of the SiC by the Al–Li matrix, since a large proportion of the droplet sizes will have developed substantial solidification structures prior to being exposed to the SiC particulates. Therefore, an alternate wetting mechanism is proposed in the present study in order to account for the observed experimental results.

During VCM processing, as already mentioned, the SiC particulates are injected at a previously selected spatial point in the atomized melt stream. At the reinforcement injection point, as shown in Table V, the SiC particulates will encounter fully solid, fully liquid, or partially solidified Al–Li droplets. The interaction of atomized droplets with SiC particulates during flight and after deposition is shown schematically in Fig. 9. SEM analysis of the presolidified, overspray powders provided experimental support to the results shown in Table V. Fig. 10 for example shows the presence of SiC particulates on the surface of presolidified Al–Li powders, approximately 25 μm in diameter. This droplet size corresponds to the d_{16} droplet diameter. Also evident from this figure is the dendritic structure formed during solidification of the powders.

In order to discuss the interaction of the SiC particulates with the partially solidified or fully liquid droplets, it is necessary to consider the surface condition of the atomized droplets. The large surface area of the fine Al droplets, in combination with the high thermodynamic stability of lithium and aluminium based oxides [61] will result in the formation of surface oxides immediately following atomization, even under highly inert conditions, such as the one used in the present study. The extent of oxidation, and other reactions on the surface of the atomized droplets will depend primarily on the temperature and chem-

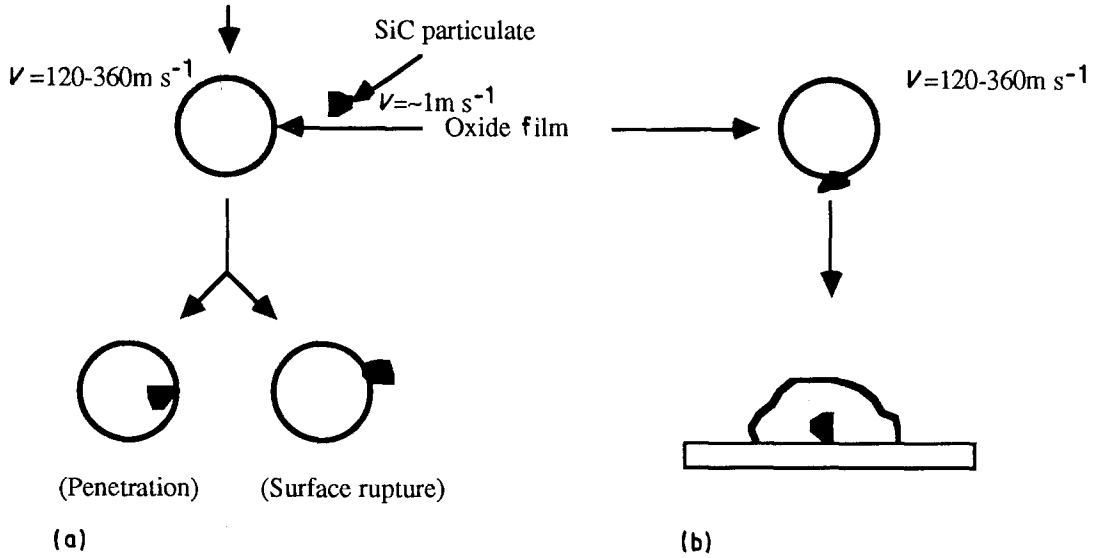

Figure 9 Types of interaction of the SiC particulates with atomized droplets during flight and after deposition. (a) Events during flight; (b) events at the substrate.

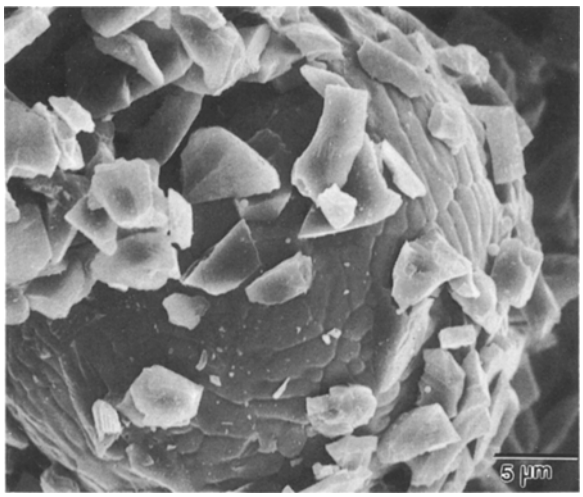

Figure 10 Presence of SiC particulates on the surface of pre-solidified Al–Li overspray powder.

ical composition of the droplets and their surrounding environments [61, 62]. On the basis of the work by Couper *et al.* [61], and taking into account the temperature of the droplets, it is possible to predict the types of oxides that will be present on the surface of the atomized droplets. The results are shown in Table V, for the three droplet sizes representing the entire distribution, and two flight distances representing the SiC injection flight distance (0.14 m) and deposition distance (0.41 m), respectively. The results shown in Table V suggest that even after assuming that all the oxygen (71 parts per million [63]) present in the droplets appears in the form of a surface oxide, the thickness of oxide will not exceed 140 nm. For the case of partially solidified, or fully liquid droplets (corresponding to 62 μm and 156 μm, in Table V), exposure of the SiC to unoxidized, molten Al–Li is probable, either during flight or after deposition. The brittle character of the aluminium oxide (γ-Al_2O_3) [61] formed on the surface of the droplets enhances the probability of rupture during impact of the SiC particulates with the atomized droplets. It is anticipated that the type of oxide present on droplets 25 μm in diameter will consist of primarily brittle and crystalline oxides (γ-Al_2O_3/γ-$LiAlO_2$) [61, 62], since the time associated with the droplet flight is only a fraction of a second. This minimizes the possibility of absorbing moisture on the oxide layer and forming stable oxides ($Al_2O_3 \cdot xH_2O/Li_2O$) as shown in Table V, for equilibrium conditions. Furthermore, the large velocity difference between the SiC particulates ($\sim$1 m/sec) and the atomized droplets (120–360 m/sec) and the impact energy during deposition will also promote rupture of any surface oxide films formed on the surfaces of the matrix droplets. Once the surface of the SiC particulates has been exposed to unoxidized, molten aluminium, the relatively high thermodynamic stability of the Al ($\Delta G^\circ \sim -921$ kJ at 660 °C) and Li ($\Delta G^\circ \sim -963$ kJ at 660 °C) oxides [64] will result in the reduction of any SiO_2 present on the surface of the SiC into Al_2O_3, or Li_2O. The formation of Al_2O_3 and/or Li_2O at the Al/SiC interface will result from the following reactions:

$$4Al^{3+} + 3SiO_2 \rightarrow 2Al_2O_3 + 3Si^{4+} \quad (7)$$

$$4Li^{1+} + SiO_2 \rightarrow 2Li_2O + Si^{4+} \quad (8)$$

In view of the above discussion, one may anticipate that the Al/SiC bond will consist of a series of layers involving Al, Si, Al_2O_3, Li_2O and SiC. The aforementioned sequence of reactions is supported by the results of EDS analyses (see Fig. 7), which revealed the presence of a high Si concentration at approximately 2 μm from the interface while Si was not detected at the matrix location, 10 μm from the interface. In related studies, Kannikeswaran and Lin [59] showed through X-ray mapping the presence of a 2 μm Si rich interaction zone, slightly darker in appearance, near the surface of SiC particulate. The absence of interfacial reaction products in the as-spray deposited material, such as Al_4C_3, can be attributed to the fast rate of heat extraction during atomization, and the absence of an extensive liquid phase after impact with the deposition substrate (see Table V). The formation of a strong interfacial bond can thus be attributed to: (a) the formation of a chemical bond between Si, O and Al atoms at the surface of SiC particulates, and (b) the ability of aluminium to form a strong bond with its oxide (Al_2O_3) at the Al/SiC interface [14]. Both of these factors effectively increase the work of adhesion, W_{ad}, and therefore contribute to the wetting behaviour observed in the present study.

The proposed mechanism accounts for the observed wetting of SiC particulates by an Al–Li matrix during VCM processing, by taking into consideration the processing history. This type of wettability, where the dynamic forces associated with the processing history play an important role in determining the extent of wetting and interfacial activity, and affect the resulting bond strength, is designated as dynamic wettability.

6. Conclusions

1. The preliminary results presented in this study suggest that the interfacial activity during VCM promoted the formation of a strong Al–Li/SiC_p bond. This was confirmed by the fracture, rather than pull-out, of the SiC particulates during deformation.

2. The results of EDS analyses conducted on fractured SiC particulates indicate that thermal conditions associated with VCM processing promotes diffusion of Al into SiC particulates.

3. The absence of interfacial reaction products in the as-spray deposited VCM material, as confirmed by TEM and SEM/EDS analyses, suggests that the temperature of the interface during deposition remained relatively low.

4. The concept of dynamic wettability is introduced to explain the wetting behaviour in Al–Li/SiC_p observed in the present study.

Acknowledgements

The authors wish to acknowledge the Army Research Office (Grant No. DAAL03-89-K-0027) and National

Science Foundation (Grant No. MSS 8957449) for their financial support; to Reynolds Metals for supplying the alloys; to Superior Graphite Co. for supplying the SiC_p; to Buehler Inc. for facilitating the image analysis; and to Mr. Irwin Sauer for his assistance with the experimental part of this study.

References

1. S. G. FISHMAN, *J. Metals* **38** (1986) 26.
2. Y. FLOM and R. J. ARSENAULT, *J. Metals* **38** (1986) 31.
3. Y. FLOM and R. J. ARSENAULT, *Mater. Sci. Engng.* **77** (1986) 191.
4. A. H. M. HOWES, *J. Metals* **38** (1986) 28.
5. A. MORTENSEN, M. N. GUNGOR, J. A. CORNIE and M. C. FLEMINGS, *J. Metals* **38** (1986) 30.
6. A. MORTENSEN, J. A. CORNIE and M. C. FLEMINGS, *J. Metals* **40** (1988) 12.
7. V. C. NARDONE and K. W. PREWO, *Scripta Metall.* **20** (1986) 43.
8. H. J. RACK, Proceedings of Sixth International Conference on Composite Materials, edited by F. L. Matthews, N. C. R. Buskell, J. M. Hodgkinson and J. Morton (Elsevier, London, 1987) p. 2.382.
9. M. RUHLE and A. G. EVANS, Materials Research Symposium Proceedings **120** (1988) 293.
10. P. K. ROHATGI, R. ASTHANA and S. DAS, *Int. Met. Rev.* **31** (1986) 115.
11. R. L. MAHAR, R. JAKASAND and C. A. BRUCH, "Behavior study of sapphire wool, aluminum and Al alloy composites" (Tech. Rep. AFML-TR-68, May 1968).
12. R. L. MEHAN and E. FEINGOLD, *J. Mater.* **2** (2) (1967) 239.
13. H. R. SHELTY and T.-W. CHOO, *Met. Trans. A.* **16** (1985) 853.
14. S. M. WOLF, A. P. LEVITT and J. BROWN, *Chem. Engng. Prog.* **62** (1966) 74.
15. F. DELANNAY, L. FROYEN and A. DERUYTTERE, *J. Mater. Sci.* **22** (1987) 1.
16. C. G. LEVI, G. J. ABASCHIAN and R. MEHRABIAN, *Met. Trans. A.* **9** (1978) 697.
17. A. BANERJEE, MSc Thesis (University of Kerala, India, 1982).
18. M. UEKI, M. NAKA and I. OKAMOTO, *J. Mater. Sci. Lett.* **5** (1986) 1261.
19. D.-J. LEE, M. D. VAUDIN, C. A. HANDWERKER and U. R. KATTNER, Materials Research Symposium Proceedings **120** (1988) 293.
20. S. R. NUTT and R. W. CARPENTER, *Mater. Sci. Engng.* **75** (1985) 169.
21. C. LEA and C. MOLINARI, *J. Mater. Sci.* **19** (1984) 2336.
22. T. MALIS and M. C. CHATURVEDI, *J. Mater. Sci.* **17** (1982) 1479.
23. Duralcan Metal Matrix Composites, May–June (1989) Data Report Package (Dural Aluminum Composites Corporation, San Diego, CA 92121).
24. T. W. CLYNE, M. G. BADER, G. R. CAPPLEMAN and P. A. HUBERT, *J. Mater. Sci.* **20** (1985) 85.
25. T. W. CLYNE and J. F. MASON, *Met. Trans.* **18** (1987) 1519.
26. J. A. CORNIE, A. MORTENSEN and M. C. FLEMINGS, Proceedings of Sixth International Conference on Composite Materials, ICCM and ECCM, edited by F. L. Matthews, N. C. R. Buskell, J. M. Hodgkinson and J. Morton (Elsevier, London, 1987) p. 2.297.
27. A. MORTENSEN, J. A. CORNIE and M. J. C. FLEMINGS, *Met. Trans.* **19** (1988) 709.
28. R. MEHRABIAN, Materials Research Society Symposium **120** (1988) 3.
29. H. L. MARCUS, D. L. BOURELL, Z. ELIEZER, C. PERSAD and W. F. WELDON, *J. Metals* **39** (12) (1987) 6.
30. J. M. PAPAZIAN, *Met. Trans.* **19** (1988) 2945.
31. S. OCHIA and K. OSAMURA, *Met. Trans.* **18** (1987) 673.
32. E. F. FASCETTA, R. G. RIEK, R. MEHRABIAN and M. C. FLEMINGS, Trans. AFS, **81** (1973) 81.
33. R. MEHRABIAN and M. C. FLEMINGS, Trans. AFS, **80** (1972) 173.
34. M. GUPTA, F. A. MOHAMED and E. J. LAVERNIA, *Materials and manufacturing processes*, **5** (1990) 165.
35. M. GUPTA, F. A. MOHAMED and E. J. LAVERNIA, in Proceedings of the International Symposium on Advances in Processing and Characterization of Ceramic Metal Matrix Composites, CIM/ICM, 17, edited by H. Mostaghaci (Pergamon Press, 1989) p. 236.
36. T. C. WILLIS, *Metals and Materials*, **4** (1988) 485.
37. C. L. BUHRMASTER, D. E. CLARK and H. O. SMART, *J. Metals* **40** (1988) 44.
38. A. R. E. SINGER, *Annals of the CIRP*, **32** (1983) 145.
39. I. A. IBRAHIM, F. A. MOHAMED and E. J. LAVERNIA, *J. Mater. Sci.* **26** (1991) 1137.
40. E. J. LAVERNIA, T. S. SRIVATSAN and F. A. MOHAMED, *J. Mater. Sci. Lett.* **25** (1990) 1137.
41. E. J. LAVERNIA and N. J. GRANT, *Intl. J. Rapid Solidif.* **2** (1986) 93.
42. M. RUHR, E. LAVERNIA and J. BARAM, *Metall. Trans. A.* **21** (1990) 1785.
43. R. H. BRICKNELL, *Met. Trans.* **17** (1986) 583.
44. Private communication with Tracor-Northern, Middleton, WI 53562.
45. E. GUTIERREZ, E. J. LAVERNIA, G. TRAPAGA, J. SZEKELY and N. J. GRANT, *Met. Trans. A* **20** (1989) 71.
46. E. J. LAVERNIA, *Intl. J. Rapid Solidif.* **5** (1989) 47.
47. R. J. ARSENAULT, *Mater. Sci. Eng.* **64** (1984) 171.
48. A. P. DIVECHA, S. G. FISHMAN and S. D. KARMARKAR, *J. Metals* **33** (1981) 12.
49. J. C. BARAM, M. K. VEISTINEN, E. J. LAVERNIA, M. ABINANTE and N. J. GRANT, *J. Mater. Sci.* **23** (1988) 2457.
50. S-Y. OH, J. A. CORNIE and K. C. RUSSELL, Ceramic Engineering Science Proceedings, **8** [7–8] (1987) 912.
51. J. E. MCDONALD and J. G. EBERHART, Trans. TMS-AIME, **233** (1965) 512.
52. V. LAURENT, D. CHATAIN and N. EUSTATHOPOULOS, *J. Mater. Sci.* **22** (1987) 244.
53. R. WARREN and C. H. ANDERSON, *Composites* **15** (1984) 101.
54. E. J. LAVERNIA, E. GUTIERREZ, J. SZEKELY and N. J. GRANT, *Intl. J. Rapid Solidif.* **4** (1988) 89.
55. R. MEHRABIAN, R. G. RIEK and M. C. FLEMINGS, *Metall. Trans. A.* **5** (1974) 1899.
56. R. J. ARSENAULT and C. D. PANDE, *Scripta Metall.* **18** (1984) 1131.
57. S. NOURBAKSH, H. MARGOLIN and F. L. LIANG, *Met. Trans.* **20** (1989) 2159.
58. J. M. YANG, W. H. KAO and C. T. LIN, *Met. Trans.* **20** (1989) 2459.
59. K. KANNIKESWARAN and R. Y. LIN, *J. Metals* (Sept. 87) 17.
60. T. ISEKI, T. KAMEDA and T. MARUYAMA, *J. Mater. Sci.* **19** (1984) 1692.
61. M. J. COUPER, M. NAUER, R. BAUMANN and R. F. SINGER, Brown Boveri Laboratory Report (Dec. 1987).
62. D. J. FIELD, G. M. SCAMANS and E. P. BUTLER, in "Aluminium–Lithium Alloys "II", edited by E. A. Starke Jr. and T. H. Sanders Jr. (April 12–14, 1983, Monterey, California) pp. 657–666.
63. J. M. MARINKOVICH, F. A. MOHAMED, J. R. PICKENS and E. J. LAVERNIA, *J. Metals* **41** (9) (1989) 36.
64. L. S. DARKEN and R. W. GURRY in "Physical Chemistry of Metals" (McGraw-Hill, New York, 1953).

Received 8 March
and accepted 2 August 1990